Correlation between dielectric and optical measurements in the smectic-C^*_α phase

R. Douali,[1] C. Legrand,[1] V. Laux,[2] N. Isaert,[3] G. Joly,[3] and H. T. Nguyen[4]

[1]*Laboratoire d'Etude des Matériaux et des Composants pour l'ELectronique, EA 2601, Université du Littoral Côte d'Opale, 50 Rue Ferdinand Buisson, B.P. 717, 62228 Calais, France*

[2]*Laboratoire de Thermophysique de la Matière Condensée, UMR CNRS 8024, MREID, Université du Littoral Côte d'Opale, 145 Avenue Maurice Schumann, 59140 Dunkerque, France*

[3]*Laboratoire de Dynamique et Structure des Matériaux Moléculaires, UMR CNRS 8024, Bâtiment P5, Université de Lille I, 59655 Villeneuve d'Ascq, France*

[4]*Centre de Recherche Paul Pascal, Université de Bordeaux I, Av. Schweitzer, 33600 Pessac, France*

(Received 8 July 2003; revised manuscript received 13 October 2003; published 31 March 2004)

We present optical and dielectric measurements in the smectic-C^*_α (SmC^*_α) phase of three homologues of an alkoxy benzoate series. Two different behaviors are observed depending on the values and the temperature evolution of the azimuthal angle difference α between two adjacent layers. For moderate values of α, the Goldstone mode is predominant over the whole SmC^*_α phase. For large values of α, we can distinguish the soft mode near the SmA^*-SmC^*_α phase transition and the Goldstone mode at lower temperatures. In this case, discontinuities are also observed at the SmC^*_α-SmA^* phase transition. These dielectric features are correlated with optical properties using simulations based on the discrete phenomenological ''clock model.''

DOI: 10.1103/PhysRevE.69.031709 PACS number(s): 61.30.−v, 64.70.Md

I. INTRODUCTION

Chiral liquid crystals exhibit a rich polymorphism between the ordered solid state and the isotropic liquid phase. The ferroelectric [smectic-C^* (SmC^*)], antiferroelectric (SmC^*_A), and intermediate phases (SmC^*_α and ferrielectric SmC^*_{FI}) present interesting optical and electroptical properties. Some of these phases are used for applications in panel display technology [1]. Numerous studies have been devoted to these phases to understand their structures [2–4]. It has been shown that the SmC^* phase is smectic (structure with layers). In each layer, the molecules are tilted with a tilt angle θ with respect to the layer normal. When we move along the layer normal, the direction of the tilt angle slowly rotates around the layer normal and a helical structure is obtained. R. B. Meyer has shown the ferroelectricity of this phase by symmetry considerations [5]. In the SmC^*_A antiferroelectric phase, molecules are also tilted with the same angle θ but they rotate in two adjacent layers with an angle of 180° around the layer normal (two-layer periodicity). Recently, P. Mach *et al.* used resonant x-ray diffraction to characterize these different smectic phases [6]. The results of this work show direct structural evidence of different phases. It has shown two-layer, three-layer, and four-layer periodicities in SmC^*_A, SmC^*_{FI1}, and SmC^*_{FI2} phases, respectively. In the SmC^*_α phase, the periodicity is incommensurate with the layer spacing.

In order to understand the structures of these phases and to explain the parameters which stabilize the different structures, several models have been proposed [7–16]. One of these models is the discrete phenomenological model clock model developed by M. Cepic *et al.* [13–16]. This model is the one which better describes the different experimental results. Recently, N. Vaupotic *et al.* used this model to theoretically study the dielectric properties of the different smectic phases in antiferroelectric liquid crystals [17]. We present in this paper a confrontation between experimental results (optical and dielectric measurements) performed on three antiferroelectric homologues of the same series and theoretical results using simulations based on the clock model.

II. OPTICAL MEASUREMENTS

A. Materials

We have studied three homologues, $n=9$, 10, and 11, of the benzoate series nFF [18] (Fig. 1). The rigid core of the molecule is made of three benzenic rings separated by two benzoate groups. Two hydrogen atoms of the first benzenic ring have been substituted with fluorine atoms (nFF). The three studied homologues exhibit the following phase sequence:

K-SmC^*_A-SmC^*_{FI1}−SmC^*_{FI2}-SmC^*-SmC^*_α-SmA^*-I.

The transition temperatures were determined on cooling (except for the K-SmC^*_A phase transition) with differential scanning calorimetry (DSC) measurements and optical observations (Table I). Let us notice that the SmC^*_α phase temperature range is different for the three compounds: it is narrow for the 11FF homologues (0.9 °C) and larger for 10FF and 9FF (2.7 and 5.2 °C, respectively). The increase of the temperature range of the SmC^*_α phase is linked to the decrease of the number n of the CH_2 groups in the nonchiral alkyl chain. Such a result has been reported on homologues of other series (10- and 11-OHFBBB1M7) [19]. This allows us to study the influence of the temperature range on the optical and the dielectric properties of the SmC^*_α phase.

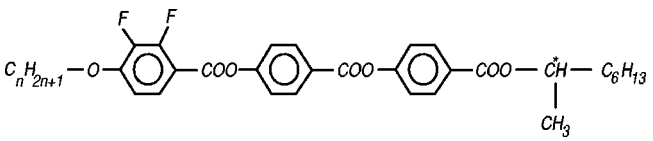

FIG. 1. Chemical formula of the benzoate series (nFF).

TABLE I. Transition temperatures (° C) for the homologues $n=9$, 10, and 11 of the benzoate series on cooling (3 °C/mn) (+ denotes temperatures obtained on heating).

	K-SmC_A^*-SmC_{FI1}^*-SmC_{FI2}^*-SmC^*-SmC_α^*-SmA^*-I						
9	71.1+	76.8	79.2	84.7	89.3	94.5	131.8
10	56.1+	91.2	92.7	95.0	100.8	103.5	130.3
11	58.8+	70.5	71.4	80.5	108.6	109.5	127.7

B. Background

We have previously studied the optical properties of the SmC_α^* phase with the purpose of identifying a special texture and to obtain evidence for some particular optical phenomena. We observed on free surface drops periodic ellipticity fringes, the so-called Friedel fringes. These fringes were the first direct observation of a helical structure in the SmC_α^* phase [20,21]. We then measured the optical period versus temperature for numerous compounds belonging to different series [22–26]. This complete study allowed us to obtain evidence for different optical period behaviors, depending on the thermal history of the sample and on the phase sequence of the compound. We showed throughout that these different behaviors are always part of a general behavior, typical of the SmC_α^* phase: this behavior is characterized by a weak optical period near the low temperature phase transition, a period divergence (interpreted as a reversal) in the phase interval, and again a weak optical period near the high temperature phase transition [26]. Figure 4(a) (for the 9FF compound) displays the typical behavior. After that we identified three categories [26], determined by the phase sequence and the pitch variations in the SmC^* phase.

(i) The first category corresponds to the compounds exhibiting a long aliphatic chain and a large SmC^* temperature range. The SmC^*-SmC_α^* transition is continuous. On heating, the compounds only display the low temperature part of the general behavior. On cooling, two behaviors have been observed: the compound exhibits either the low temperature part of the general behavior (reversible evolution) or the whole general behavior. 11FF belongs to this category.

(ii) The second category corresponds to the compounds with an intermediate length of aliphatic chain, and a short SmC^* temperature range. In this case the SmC^*-SmC_α^* transition is discontinuous. The optical period variations are reversible; one can observe the whole general behavior, for a larger SmC_α^* temperature range, or only its low temperature part, for a shorter SmC_α^* temperature range. 9FF and 10FF belong to this category.

(iii) The third category concerns the compounds exhibiting a short aliphatic chain, and no SmC^* in the sequence. On cooling the whole general behavior is always observed, but on heating the optical period evolution depends on the low temperature phases formed before.

To correlate the optical period variations with the SmC_α^* phase structure, we compared the general behavior with structural models proposed in the literature. We concluded that the model proposed by B. Zeks and M. Cepic [13–16] seems to be in good agreement with our experimental results.

In this paper, we remind the reader of the methods used to measure the helical pitch and the fringe period. Both methods have been precisely described before. We report the experimental results for the three compounds studied by optical means. The azimuthal angle difference α variations versus temperature are then determined using optical models of helical phases.

C. Experimental procedure

We performed pitch measurements in the SmC^* and SmC_A^* phases and optical period measurements in the SmC_α^* phase. Samples were placed in a Mettler FP5 hot stage, and observed using an Ortholux Leitz polarizing microscope in the reflection mode.

In the SmC^* and SmC_A^* phases, we used the Grandjean-Cano method [20,25] to perform the helical pitch measurements. The liquid crystal is introduced into a prismatic cell made of two glass slides; a step lattice, produced by the edge dislocations then appears. The lattice period is equal to one half pitch in the SmC_A^* phase, and one full pitch in the SmC^* phase. If the pitch range allows it, selective reflection colors are visible: $\lambda = np$ and $\lambda = 2np$ for the SmC^* phase, where λ is the reflected wavelength, n the average refractive index ($n=1.5$), and p the helical pitch.

In the SmC_α^* phase, we observed free surface drops. When the studied phase is helical, this kind of sample displays Friedel fringes. We thus were able to measure this fringe optical period L versus temperature. Next, the pitch p is deduced from the optical period L, and simultaneously the azimuthal angle difference $\alpha = 2\pi d/p$, where d is the layer thickness.

The relation between p and L is simple in two cases:

(i) $|\alpha| \lesssim \pi/4$ (synclinic organization); according to the de Vries theory, the double optical period $2L$ is very close to the pitch p:

$$2L \simeq p. \tag{1}$$

(ii) $\pi > \alpha \gtrsim 3\pi/4$ (anticlinic organization). The double period is then very close to the helical pitch of the bilayer structure:

$$2L \simeq p_{AF}. \tag{2}$$

In this case, the azimuthal angle difference α obeys

$$\alpha - \pi = \frac{2\pi d}{p_{AF}}. \tag{3}$$

The two previous situations typically happen for most SmC^* (i) and SmC_A^* phases (ii); but for the SmC_α^* phase, a third case can occur:

(iii) $\pi/4 \lesssim \alpha \lesssim 3\pi/4$. In this case, the structure can no longer be considered as a continuous helix, and the de Vries theory can no longer be applied. The correlation between L and α is more complicated: a calculation based on the

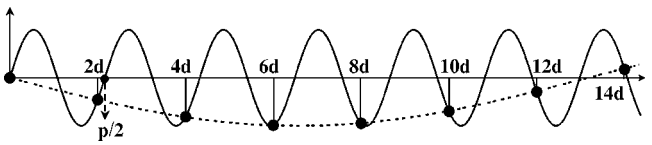

FIG. 2. Ellipticity oscillations versus sample thickness "sinusoid with a period equal to $p/2$" (solid line). Ellipticity observed on samples in which the thickness grows bilayer by bilayer (dotted line with some points).

Reusch stacks model has been performed by L. Détré [27]. The double optical period is then no longer equal to the pitch, but to

$$2L = 4d\left(\frac{1}{\frac{p}{4d}-1}+1\right) = 4d\left(\frac{1}{\frac{\pi}{2\alpha}-1}+1\right). \qquad (4)$$

The theory of Reusch stack cannot be given here: we send back to Joly's works [28–30]; we simply explain Eq. (4) in a schematic manner. In Fig. 2 are drawn ellipticity oscillations of polarized reflected light versus the thickness of the sample. These oscillations have a period that coincides with the half pitch, but they are observed on drop samples in which the thickness grows bilayer by bilayer [31] so the ellipticity oscillations appear to have a superperiod L much larger than $p/2$. Figure 3 represents the optical period evolution versus α given in Eq. (4). Let us notice that in Eq. (4) L diverges for $\alpha=\pi/2$ $(p=4d)$ and that this divergence also clearly appears in Fig. 2 if making $p/2\rightarrow 2d$.

D. Results

We shall now report the optical measurements for the 9FF, 10FF, and 11FF compounds of the benzoate series. The 11FF compound belongs to the first category (large SmC^* temperature range and long aliphatic chain), whereas 9FF and 10FF belong to the second category (SmC^* short temperature range and intermediate length of aliphatic chain). Figure 4 displays the optical period evolution and the azimuthal angle difference variations versus temperature for the three studied compounds.

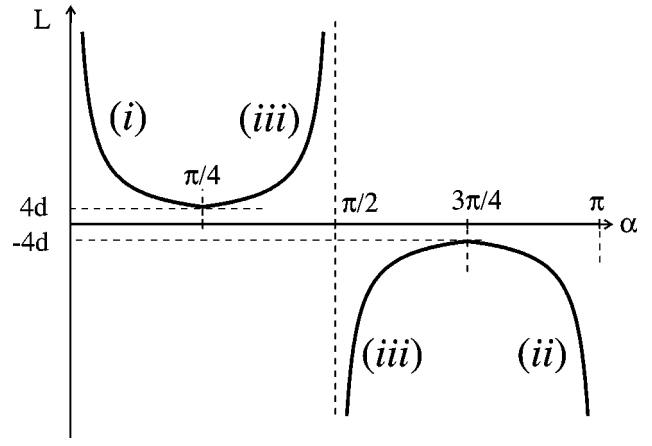

FIG. 3. Optical period L versus α. The optical period L diverges for $\alpha=\pi/2$ [case C*iii*, formula (4)]. Branches (i) and (ii) correspond to the values $\alpha\lesssim\pi/4$ and $\alpha\gtrsim 3\pi/4$ (cases C*i*, C*ii*).

1. 11FF compound: First category

In the SmC_A^* phase, the pitch is about 0.43 μm and does not vary with temperature. The liquid crystal is red $(\lambda=np)$. In the SmC^* phase, the pitch increases from 0.37 μm at 85 °C to 0.39 μm at 106.5 °C. On heating the pitch falls from 0.39 μm at 106.5 °C to 0.2 μm at 108.7 °C. The liquid crystal is orange on the plateau $(\lambda=np)$, and reflects green, blue, violet $(\lambda=np)$, and red $(\lambda=2np)$ on heating. Figure 4(e) displays the optical period evolution versus temperature in the SmC^* and SmC_α^* phases. On heating the optical period exhibits only the low temperature part of the general behavior given in Fig. 3 (i). The SmC^*-SmC_α^* phase transition occurs at 108.7 °C. The Friedel fringes are already tightening in SmC^*, and go on tightening in the SmC_α^* phase up to 109.8 °C. Then they move apart, and become motionless at 110.1 °C, corresponding to the SmC_α^*-SmA* phase transition. Figure 4(f) displays α versus temperature for the 11FF compound. For this compound, the α angle ranges between 7.2° and 24°, but never crosses 90° on heating.

2. 9FF and 10FF compounds: Second category

The two compounds display the same pitch behavior in SmC^* and SmC_A^* phases; we thus report the pitch behavior only for the 10FF homologues. In the SmC_A^* phase, the pitch is about 0.41 μm and does not vary. The liquid crystal is red $(\lambda=np)$. In the SmC^* phase, the pitch is about 0.46 μm and does not vary. The liquid crystal is red $(\lambda=np)$. The SmC^*-SmC_α^* phase transition occurs with a discontinuity and a period fall is observed. This period fall is larger for the 9FF compound. On heating, the Friedel fringes form in the transition front. They are very tightened just after the transition and move apart when the temperature increases. In the SmC_α^* phase, the behaviors are different for the compounds:

(i) Figure 4(a) displays the optical period evolution for the 9FF compound. The SmC_α^* phase range is over about 8 °C, and we observed the complete general behavior: the transition occurs at 88 °C, with a front crossing the sample. The optical period decreases suddenly, reaching 0.03 μm at 90.3 °C. It then increases, diverges, and reverses at 94 °C, and increases again. This evolution is reversible. After the reversal, the fringes tightening is very fast and we are not able to perform precise measurements. We only obtain the qualitative behavior given in the figure by dotted lines. The divergence and the reversal of the optical period near 94 °C is nevertheless undoubted. It is the clear signature that the azimuthal angle difference α crossed 90° (see C*iii*). It allows us to get the range of the azimuthal angle difference α. In Fig. 4(b), are given the α values calculated with formula (4): this angle is large (64° at 90.3 °C) and increases on heating (80° at 94 °C). It crosses 90° near the SmC_A-SmC_α^* phase transition.

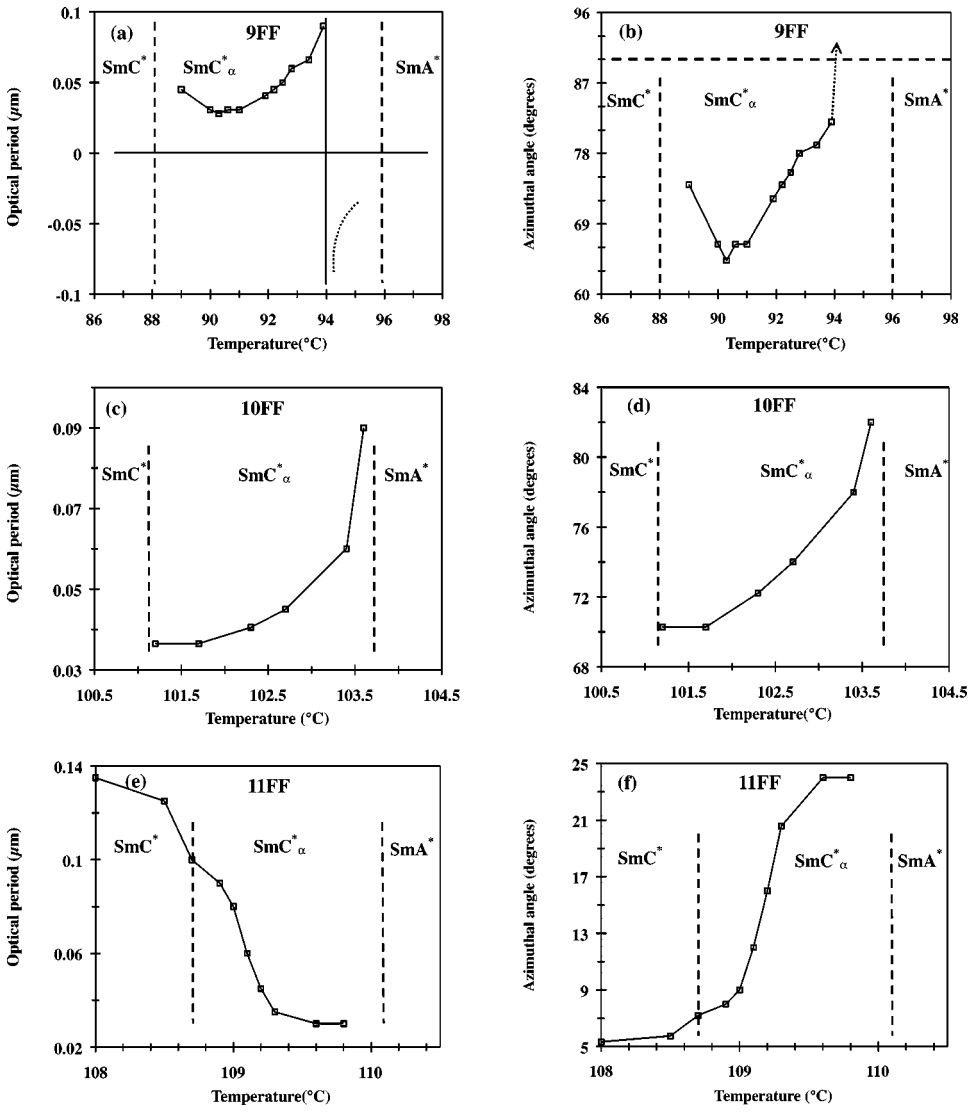

FIG. 4. Optical period and azimuthal angle difference in the compounds 9FF, 10FF, and 11FF.

(ii) Figure 4(c) displays the period evolution for the 10FF compound. The SmC^*_α phase ranges over about 3 °C, and the period only follows the low temperature part of the general behavior: it decreases (to 0.036 μm) just after the transition, and increases (up to 0.09 μm) then regularly without any divergence nor reversal. On cooling, the period is a little bigger, but displays the same evolution. For the 10FF compound, α is rather large at the SmC^*-SmC^*_α phase transition (70°); it increases with temperature, but remains always lower than 90°.

For $n=11$, the SmC^*-SmC^*_α transformation is continuous, probably without any transition (like for the liquid-gas transformation above the critical point); the pitch decreases continuously from its value in the SmC^* phase, to reach rather low values of about 15 layers. This behavior, usual for large chain compounds with a large temperature range SmC^* phase and narrow SmC^*_α one, has already been observed by several methods: direct optical observations [25,26,32]; ellipsometry [33]; resonant x-ray scattering [34].

Whereas, for 9FF and 10FF, the SmC^*-SmC^*_α transformation is first order, the pitch is discontinuous and is very short in the SmC^*_α: a few layers; the azimuthal angle difference, for 9FF crosses the $\pi/2$ value (four layers). This behavior is usual for intermediate chain length compounds, with a short SmC^* phase and larger SmC^*_α one [6,25,26,35].

III. DIELECTRIC MEASUREMENTS

A. Experimental procedure

The measuring cell consists of a planar capacitor made of two ITO (indium tin oxide) (5 Ω per square) coated glass plates (13×14 mm). The layers have been etched to obtain 5-mm-wide strip lines. The cell thickness was fixed to 22 μm with mica spacers. After superimposition of the glass plates, the active part sizes are 5×5 mm. This configuration allows us to perform measurements only in the well orientated part of the sample. The liquid crystal is introduced by capillarity in the SmA^* or the isotropic phase. A planar orientation of the sample is obtained with PVA (polyvinylalcohol) coating and rubbing. This orientation is checked with a polarizing

microscope. The electrical contact on the ITO layers is made with coaxial connectors [SMA (subminiature version A) standard]. The temperature of the sample is stabilized better than 0.01 °C using an Oxford Instrument ITC601 temperature controller. Dielectric measurements were performed in the frequency range 20 Hz–1 MHz with a HP4284A impedance analyzer. The real and imaginary parts of the complex permittivity are calculated from the measured capacitance C_m and conductance G_m:

$$\epsilon' = C_m / C_0, \tag{5}$$

$$\epsilon'' = G_m / (2\pi F C_0), \tag{6}$$

where F is the frequency and C_0 is the empty cell capacitance measured before filling. The measuring ac voltage was fixed to 0.1 V rms. The experimental setup is completely controlled with a personal computer and HPVEE software.

B. Results

We report dielectric measurements for the three compounds in SmA*, SmC^*_α, and SmC* phases (Figs. 5 and 6). In these phases, the measured dielectric spectra show only one relaxation process. So, to analyze the results, the dielectric spectra were fitted with the following formula using MATHCAD software:

$$\epsilon^* = \epsilon' - i\epsilon'' = \epsilon_\infty + \frac{\Delta\epsilon}{1 + i(F/F_C)^{(1-\beta)}} - i\frac{\sigma}{2\pi F \epsilon_0}, \tag{7}$$

where ϵ_∞ is the permittivity at a high frequency, $\Delta\epsilon$, F_C, and β are, respectively, the dielectric strength, the critical frequency, and the distribution factor of the relaxation process, σ and ϵ_0 are the conductivity and the vacuum permittivity. The value of the distribution factor β obtained after fitting is low in the SmA*, SmC^*_α, and SmC* phases ($\beta < 0.15$). This result shows that the observed relaxation is linked to one process in the SmA*, SmC^*_α, and SmC* phases.

The dielectric behaviors obtained in the SmA* and SmC* phases are similar for the three compounds. However, differences have been observed in the SmC^*_α phase. These behaviors are detailed below.

1. SmA and SmC* phases*

In the SmA* phase, the relaxation process presents a high critical frequency and a low dielectric strength. This relaxation corresponds to the soft mode linked to the amplitude fluctuations of the tilt angle θ [36]. On cooling, the critical frequency F_C and the reversed dielectric strength $\Delta\epsilon^{-1}$ linearly decrease versus temperature as predicted by theoretical models [37]. Table II shows the slopes of the curves $F_C(T)$ and $\Delta\epsilon^{-1}(T)$. These slopes are similar in the 9FF and 10FF (28 kHz/ °C and 0.028/ °C). However, the slopes are higher in the SmA* phase of the 11FF homologues (52 kHz/ °C and 0.058/ °C).

For the 11FF compound, changes in the slopes of the curves $F_C(T)$ and $\Delta\epsilon^{-1}(T)$ are observed, we attributed these changes to the SmA*-SmC^*_α and SmC^*_α-SmC* phase transitions. Let us notice that the temperature range corresponds to the one determined by DSC measurements. The behavior is similar for 9FF and 10FF compounds with dis-

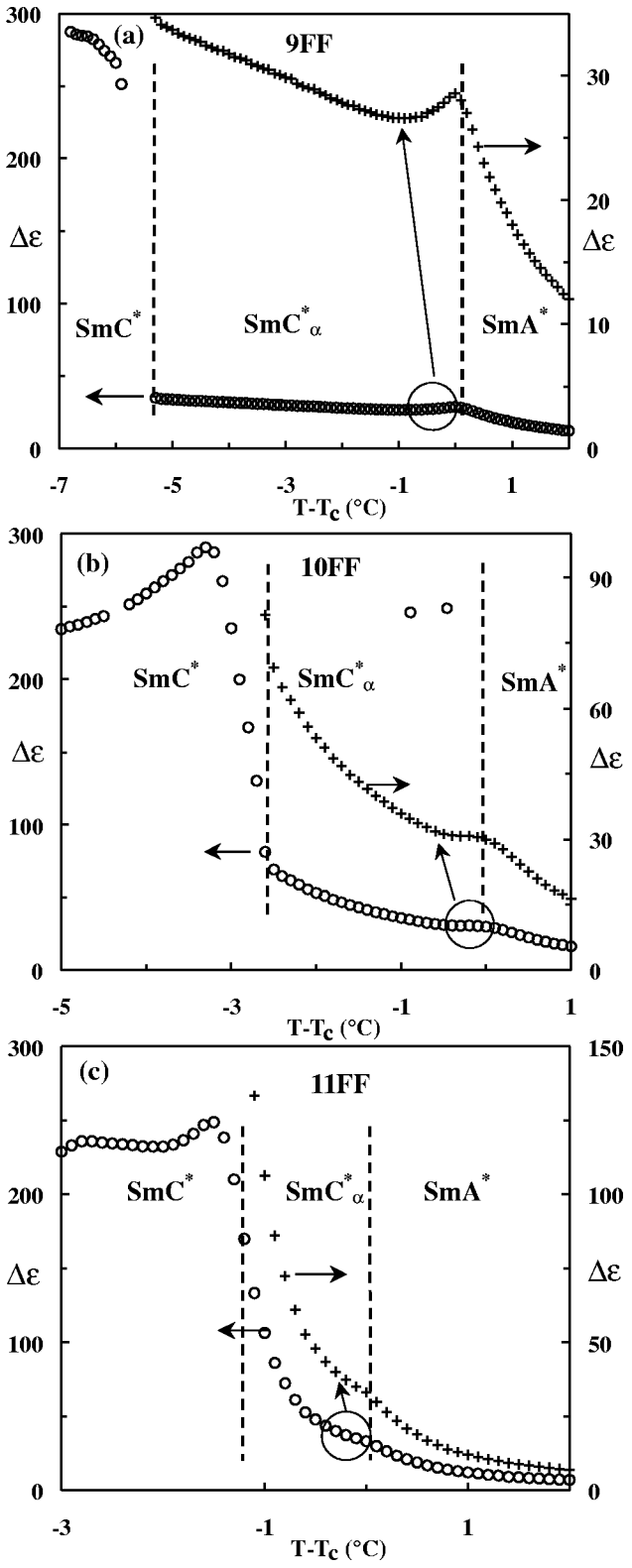

FIG. 5. Dielectric strength in the SmA*, SmC*, and SmC^*_α phases of three homologues 9FF, 10FF, and 11FF.

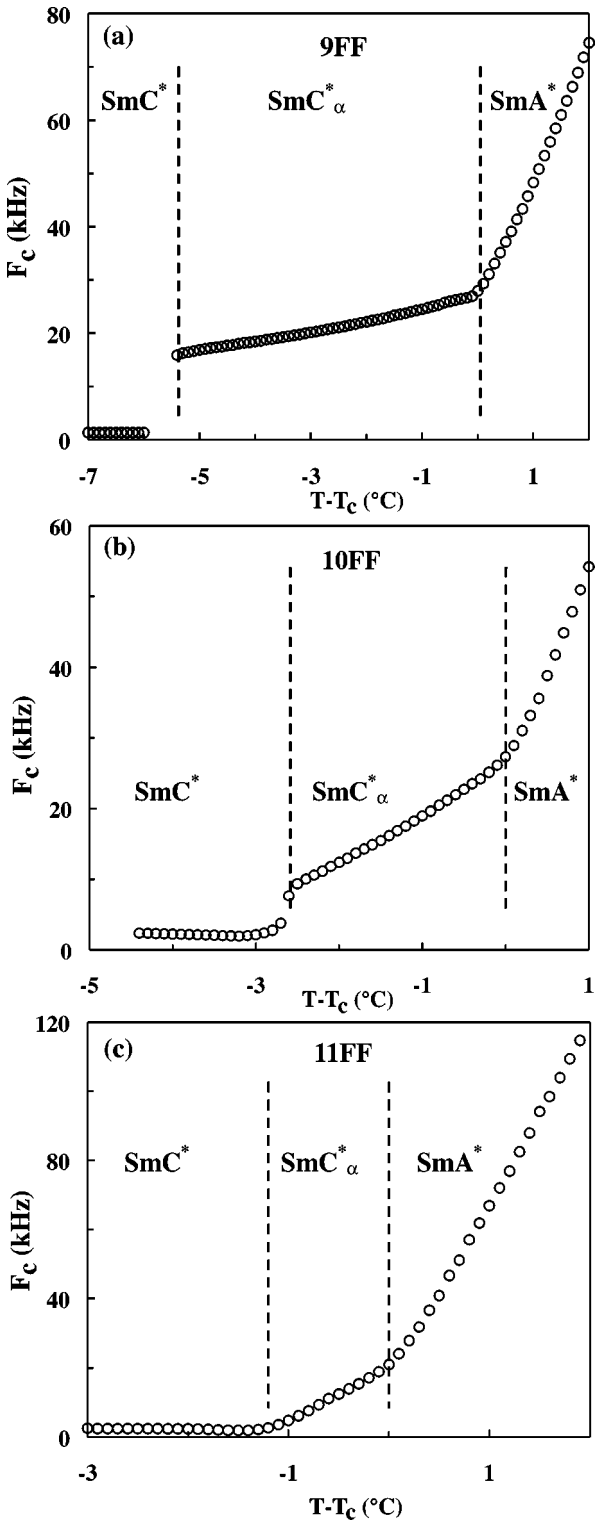

FIG. 6. Critical frequency in the SmA*, SmC*, and SmC^*_α phases of three homologues 9FF, 10FF, and 11FF.

continuities of $F_C(T)$ and $\Delta\epsilon^{-1}(T)$ at the SmC^*_α-SmC* phase transitions.

At the SmA*-SmC^*_α phase transition, the relaxation process presents the same properties in the three compounds ($\Delta\epsilon \approx 30$, $F_C \approx 25$ kHz). In the SmC* phase of the three homologues, the process presents a high dielectric strength and a low critical frequency. This relaxation corresponds to the Goldstone mode linked to the phase fluctuations of the tilt angle θ [36]. Except near the SmC^*_α-SmC* phase transition, the properties of the Goldstone mode depend slightly on the temperature and are of the same order of magnitude for the three compounds ($\Delta\epsilon \approx 250$, $F_C \approx 2$ kHz).

TABLE II. Slopes of the $F_C(T)$ and $\Delta\epsilon^{-1}(T)$ curves in the SmA* and SmC^*_α phases of the homologues 9FF, 10FF, and 11FF.

	SmA* phase		SmC^*_α phase	
	$\Delta\epsilon^{-1}(T)$	$F_C(T)$	$\Delta\epsilon^{-1}(T)$	$F_C(T)$
9FF	0.028/ °C	27.9 kHz/ °C	0.0019/ °C	1.91 kHz/ °C
10FF	0.028/ °C	27.8 kHz/ °C	0.0075/ °C	7.61 kHz/ °C
11FF	0.058/ °C	51.78 kHz/ °C	0.02/ °C	14.72 kHz/ °C

2. SmC^*_α phase

The critical frequency F_C and the dielectric strength $\Delta\epsilon$ of the relaxation process observed in the SmC^*_α phase of the 11FF homologues do not present discontinuities at the SmA*-SmC^*_α and SmC^*_α-SmC* phase transitions. The critical frequency F_C and the reversed dielectric strength $\Delta\epsilon^{-1}$ in the SmC^*_α phase presents linear decrease versus temperature but the slopes are weaker than those of the SmA* soft mode (see Table II).

In the SmC^*_α phase of 9FF homologues and except near the SmA*-SmC^*_α and SmC^*_α-SmC* phase transitions, the process evolution is similar to the one observed in the SmC^*_α phase of the 11FF: linear decreases of $F_C(T)$ and $\Delta\epsilon^{-1}(T)$. The slopes are lower than those obtained in the SmC^*_α of the 11FF compound. The dielectric behavior is different near the SmA*-SmC^*_α and SmC^*_α-SmC* phase transitions:

(i) At the SmA*-SmC^*_α phase transition, the dielectric strength $\Delta\epsilon$ presents a maximum then it decreases with temperature and a minimum is observed at about $T_C - 1$ °C. The critical frequency F_C in the SmC^*_α phase is temperature independent over 0.4 °C and then slightly decreases (Table II).

(ii) Near the SmC^*_α-SmC* phase transition, strong variations (discontinuities) of the dielectric strength and of the critical frequency versus temperature are observed.

In the SmC^*_α phase of 10FF homologues, the behavior is similar to the one of the 9FF; but the decrease of $\Delta\epsilon$ near the SmA*-SmC^*_α phase transition and the discontinuities at the SmC^*_α-SmC* phase transition are less pronounced compared to 9FF compound.

IV. DISCUSSION

A. Theoretical model

The discrete phenomenological model clock model proposed by M. Cepic *et al.* has been previously described in

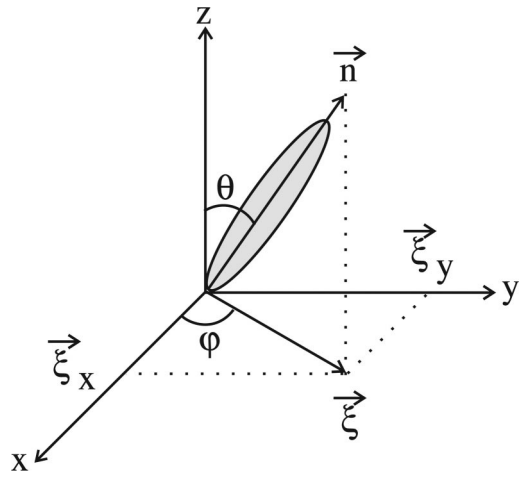

FIG. 7. Order parameter in chiral smectic phases.

several papers [13–17]. In this section, we only give the main results of the model. In the next section, we present numerical simulations used to discuss the dielectric properties of the SmC_α^* phase.

In the basic version of the clock model, the free energy is given by the following equation:

$$G=\sum_j \left(\frac{a_0}{2}\vec{\xi}_j^2+\frac{b_0}{4}\vec{\xi}_j^4+\frac{a_1}{2}(\vec{\xi}_j\cdot\vec{\xi}_{j+1}) + \frac{a_2}{8}(\vec{\xi}_j\cdot\vec{\xi}_{j+2})+\frac{f}{2}(\vec{\xi}_{j+1}\times\vec{\xi}_j)_z \right), \tag{8}$$

where

$$\vec{\xi}_j=(\theta\cos j\alpha,\theta\sin j\alpha). \tag{9}$$

$\vec{\xi}_j$ is the order parameter which describes the magnitude and the direction of the molecular tilt of the jth layer with respect to the layer normal (z axis) (Fig. 7). θ stands for the tilt angle amplitude and α for the azimuthal angle difference between two adjacent layers. The parameter a_0 depends on the temperature:

$$a_0=a(T-T_0), \tag{10}$$

where a is a positive parameter and T_0 the transition temperature for the achiral compound. For a second order transition, the parameter b_0 should be positive. The interactions with the nearest-neighboring and next-nearest-neighboring layers interactions are taken into account via the parameters a_1 and a_2. The term with the coefficient f describes the chiral interactions which are supposed negligible with respect to the other terms. Using the parameters θ and α, the free energy can also be written as follows:

$$G=\sum_j \left(\frac{a_0}{2}\theta^2+\frac{b_0}{4}\theta^4+\frac{a_1}{2}\theta^2\cos\alpha + \frac{a_2}{8}\theta^2\cos 2\alpha+\frac{f}{2}\theta^2\sin\alpha \right). \tag{11}$$

By minimizing the free energy with respect to θ and α, M. Cepic *et al.* obtained different stable solutions corresponding to the structures in different phases. The structure proposed for the SmC_α^* phase corresponds to the case

$$\alpha\approx\arccos\left(\frac{-a_1}{a_2}\right). \tag{12}$$

The azimuthal angle difference is temperature independent in this model. The azimuthal angle difference results of the competition between nearest-neighboring and next-nearest-neighboring layers interactions. In the SmC_α^* phase, the next-nearest-neighboring layers interactions are antiferroelectric and dominate the interactions. The azimuthal angle difference takes relatively high values explaining the small resulting helical pitch.

The model has been recently extended by N. Vaupotic *et al.* to study dielectric properties of different chiral phases. The procedure used by the authors is well described in previous papers [17]. In the SmC_α^* phase, two dielectric relaxation processes are predicted: the soft and Goldstone modes. The theoretical formulas versus α of the dielectric strength and the critical frequency of the two processes are

$$\omega_{G,S}=\frac{A(\alpha)+B(\alpha)\pm\sqrt{[A(\alpha)+B(\alpha)]^2-4[A(\alpha)B(\alpha)-C(\alpha)^2]}}{2\gamma}, \tag{13}$$

$$\Delta\epsilon_G=\frac{K'}{\omega_G}\left(1-\frac{2C(\alpha)}{\gamma(\omega_S-\omega_G)}\right), \tag{14}$$

$$\Delta\epsilon_S=\frac{K'}{\omega_S}\left(1+\frac{2C(\alpha)}{\gamma(\omega_S-\omega_G)}\right), \tag{15}$$

where

$$A(\alpha)=a_0+3b_0\theta^2+a_1\cos^2(\alpha)+\frac{a_2}{4}\cos^2(2\alpha) + f\cos(\alpha)\sin(\alpha), \tag{16}$$

$$B(\alpha)=a_0+b_0\theta^2+a_1\cos^2(\alpha)+\frac{a_2}{4}\cos^2(2\alpha) + f\cos(\alpha)\sin(\alpha), \tag{17}$$

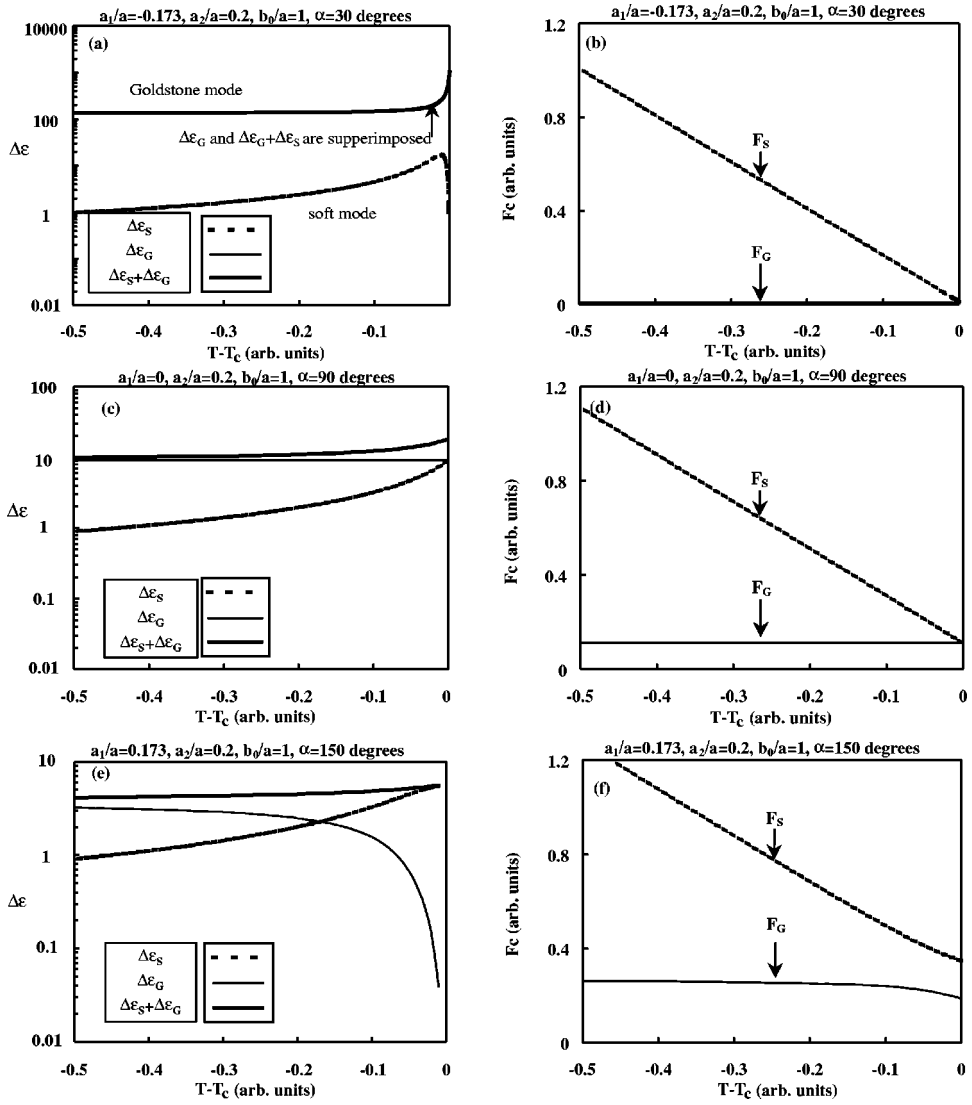

FIG. 8. Dielectric strength and critical frequency of the relaxation processes predicted by the discrete phenomenological model in the SmC_α^* phase for different cases of the azimuthal angle difference α.

$$C(\alpha)=a_1\sin^2(\alpha)+\frac{a_2}{4}\sin^2(2\alpha)-f\cos(\alpha)\sin(\alpha). \tag{18}$$

Using the formulas given above and choosing the adequate parameters, we can study the influence of the α angle on the dielectric properties of the SmC_α^* phase.

B. Simulations

In order to explain the behavior's difference experimentally observed in the three compounds (see Sec. III), we simulated the temperature evolution of the dielectric strength and the critical frequency using Eqs. (13)–(18). The temperature variation is taken into account via the parameter a_0/a [Eq. (10)]. In these simulations we also studied the influence of the parameter α which transduces the ratio between the interactions with the nearest and next-nearest layers [Eq. (12)]. The coefficient f has been chosen equal to zero because the chiral interactions are negligible with respect to the other terms.

For a given material, the signs and the values of different parameters are not arbitrary, they depend on the phase sequence of the compound, the phase transition temperatures, and on the values of the tilt angle at the different phase transitions [16,17]. In our simulations, we use the values used by N. Vaupotic in the basic version of the model; let us notice that these values are slightly different from those obtained by M. Skarabot *et al.* using birefringence and tilt angle measurements for the MHPOBC compound. This compound and those studied in this paper present the same phase sequence. Different values of the parameter a_1 have been used in order to take into account the evolution of the azimuthal angle difference α versus temperature [Eq. (13)].

The results presented in Fig. 8 show the theoretical predictions of the dielectric strength and the critical frequency evolutions versus temperature for different values of the azi-

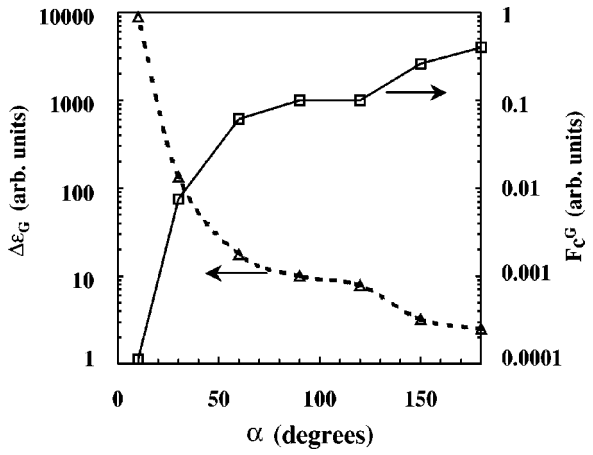

FIG. 9. Evolution of the dielectric strength and the critical frequency of the Goldstone mode in the SmC^*_α phase at low temperatures versus the azimuthal angle difference α.

muthal angle difference α between two adjacent layers. For moderate values of α (30°), the theoretical predictions in the SmC^*_α phase are similar to those predicted by the model of the SmC^*-SmA^* phase transition [37]: on heating, the dielectric strength of the soft mode increases and the critical frequency decreases. The Goldstone mode is predominant in all the SmC^*_α phase and presents a larger dielectric strength and a lower critical frequency. In this case, the soft mode cannot be observable without applying a dc bias. When the azimuthal angle difference α increases, the dielectric strength of the Goldstone mode decreases and the soft mode contribution is no longer negligible. The two dielectric strengths are equal in the case α=90°. For larger values of α [Figs. 8(e) and (f)], the Goldstone mode is weaker and the soft mode becomes predominant near the SmA^*-SmC^*_α phase transition. So, summarizing the results of simulations, we differentiate two different cases: the first case, ''high values of α'' corresponds to a predominant Goldstone mode at low temperatures and a predominant soft mode near the SmA^*-SmC^*_α phase transition; in the second case, ''moderate values of α,'' the Goldstone mode is predominant over the whole SmC^*_α domain.

Using the simulated values at lower temperatures where the Goldstone mode is predominant, we can also study the evolution of this mode in the SmC^*_α phase versus the azimuthal angle difference α. Figure 9 shows that when α decreases (pitch increases), the dielectric strength and the critical frequency of the Goldstone mode increases and decreases, respectively. This result is similar to the one predicted in the SmC^* phase by the model of the SmC^*-SmA^* phase transition [37]. Let us notice that the azimuthal angle difference α is temperature dependent, then Fig. 9 also presents a qualitative evolution of $\Delta\epsilon$ and F_C versus temperature.

C. Discussion

In this section, we qualitatively explain the optical and dielectric behaviors for the different compounds.

In the 11FF compound, relatively low values of the azimuthal angle difference α were obtained by optical measurements ($7°<\alpha<25°$). Such values of α correspond to the simulated case ''moderate values of α,'' where only one relaxation process (Goldstone mode) is predominant over the whole SmC^*_α range. So, we attribute the relaxation process observed in the 11FF compound to the Goldstone mode. This attribution is in agreement with previously published results showing that, under a dc bias, the process of the SmC^*_α phase is strongly modified and a soft mode behavior is observed [38]. The increase of $\Delta\epsilon$ (Fig. 5) and the decrease of F_C (Fig. 6) on cooling over the whole SmC^*_α range are connected with the temperature dependence of the angle α as predicted by simulations (Fig. 9). Furthermore, the continuities of $\Delta\epsilon$ and F_C at the SmC^*-SmC^*_α transition are explained by the continuity of the angle α observed by means of optical measurements at this transition [Fig. 4(f)].

In the 10FF and 9FF compounds, the temperature dependencies of the angle α are different from the one of the 11FF compound:

(i) The values of α are higher [Figs. 4(b) and (d)] and correspond for the simulated case ''high values of α'' [Figs. 8(e) and (f)]. For the 9FF compound, α crosses 90° near the SmA^*-SmC^*_α phase transition [Fig. 4(b)].

(ii) Discontinuities of α are observed at the SmC^*-SmC^*_α transition.

In the case ''high values of α,'' the model predicts that the Goldstone mode is still observed in the SmC^*_α phase excepted near the SmC^*_α-SmA^* transition where the soft mode becomes predominant. So, the following qualitative interpretation can be proposed for the dielectric results in the 10FF and 9FF compounds.

(i) Near the SmC^*_α-SmA^* transition (over 1 °C), the observed relaxation process corresponds to the soft mode. As predicted by simulations, the dielectric strength $\Delta\epsilon$ is maximum at the SmC^*_α-SmA^* transition and decreases versus temperature [Fig. 5(a)]. However, no increase but only a plateau of F_C is observed with decreasing temperature.

(ii) At lower temperatures, the relaxation process is connected with the Goldstone mode with discontinuities of $\Delta\epsilon$ and F_C at the SmC^*-SmC^*_α phase transition. Such discontinuities are in agreement with the α angle temperature dependencies (see Sec. II D).

Let us notice that the effect of a dc bias on the dielectric properties of 9FF and 10FF compounds is different from the one observed on the 11FF compound: $\Delta\epsilon$ is strongly modified only at low temperatures [39].

V. CONCLUSION

We have shown qualitative agreement between optical, dielectric measurements and the clock model. The values and the temperature dependence of the azimuthal angle difference α are important parameters to better understand the dielectric behavior of the SmC^*_α phase. Let us notice that the

angle α results of the competition between nearest-neighboring and next-nearest-neighboring layers interactions. It would be interesting to introduce the temperature dependence of the parameters in the model [16].

ACKNOWLEDGMENT

A part of this work was supported by the Conseil Régional Nord Pas de Calais.

[1] N. Clark and S.T. Lagerwall, Appl. Phys. Lett. **36**, 899 (1980).
[2] A.D.L. Chandani, Y. Ouchi, H. Takezoe, A. Fukuda, K. Terashima, K. Furukawa, and A. Kishi, Jpn. J. Appl. Phys., Part 2 **28**, L1261 (1989).
[3] E. Gorecka, A.D.L. Chandani, Y. Ouchi, H. Takezoe, and A. Fukuda, Jpn. J. Appl. Phys., Part 1 **29**, 131 (1990).
[4] Y. Takanishi, K. Hiraoka, V.K. Agraval, H. Takezoe, A. Fukuda, and M. Matsushita, Jpn. J. Appl. Phys., Part 1 **30**, 2023 (1991).
[5] R.B. Meyer, Mol. Cryst. Liq. Cryst. **40**, 33 (1977).
[6] P. Mach, R. Pindak, A.M. Levelut, P. Barois, H.T. Nguyen, C.C. Huang, and L. Furenlid, Phys. Rev. Lett. **81**, 1015 (1998).
[7] T. Isozaki, K. Hiraoka, Y. Takanishi, H. Takezoe, A. Fukuda, Y. Suzuki, and I. Kawamura, Liq. Cryst. **12**, 59 (1992).
[8] T. Isozaki, T. Fujikawa, H. Takezoe, A. Kukuda, T. Hagiwara, Y. Suzuki, and I. Kawamura, Phys. Rev. B **48**, 13 439 (1993).
[9] H. Orihara and Y. Ishibashi, Jpn. J. Appl. Phys., Part 2 **29**, L115 (1990).
[10] V.L. Lorman, A.A. Bulbitch, and P. Toledano, Phys. Rev. E **49**, 1367 (1994).
[11] V.L. Lorman, Mol. Cryst. Liq. Cryst. Sci. Technol., Sect. A **A 262**, 437 (1995).
[12] V.L. Lorman, Liq. Cryst. **20**, 267 (1996).
[13] B. Zeks and M. Cepic, Liq. Cryst. **14**, 445 (1993).
[14] M. Cepic and B. Zeks, Mol. Cryst. Liq. Cryst. Sci. Technol., Sect. A **A 61**, 263 (1995).
[15] M. Cepic and B. Zeks, Liq. Cryst. **20**, 29 (1996).
[16] M. Skarabot, M. Cepic, B. Zeks, R. Blinc, G. Heppke, A.V. Kityk, and I. Musevic, Phys. Rev. E **58**, 575 (1998).
[17] N. Vaupotic, M. Cepic, and B. Zeks, Ferroelectrics **245**, 185 (2000).
[18] V. Faye, J.C. Rouillon, C. Destrade, and H.T. Nguyen, Liq. Cryst. **19**, 47 (1995).
[19] A. Cady, D.A. Olson, X.F. Han, H.T. Nguyen, and C.C. Huang, Phys. Rev. E **65**, 030701 (2002).
[20] M. Brunet and N. Isaert, Ferroelectrics **84**, 25 (1988).
[21] V. Laux, N. Isaert, H.T. Nguyen, P. Cluzeau, and C. Destrade, Ferroelectrics **179**, 25 (1996).
[22] V. Faye, H.T. Nguyen, V. Laux, and N. Isaert, Ferroelectrics **179**, 9 (1996).
[23] V. Faye, A. Babeau, F. Placin, H.T. Nguyen, P. Barois, V. Laux, and N. Isaert, Liq. Cryst. **21**, 485 (1996).
[24] V. Laux, Ph.D. thesis, Universite de Lille I, 1997.
[25] V. Laux, N. Isaert, H.T. Nguyen, and G. Joly, Liq. Cryst. **26**, 361 (1999).
[26] V. Laux, N. Isaert, V. Faye, and H.T. Nguyen, Liq. Cryst. **27**, 81 (2000).
[27] L. Dété́r, Ph.D. thesis, Universite de Lille I, 1999.
[28] G. Joly and J. Billard, J. Opt. (Paris) **13**, 227 (1982).
[29] G. Joly and N. Isaert, J. Opt. (Paris) **16**, 203 (1985).
[30] G. Joly and N. Isaert, J. Opt. (Paris) **17**, 211 (1986).
[31] D.R. Link, G. Natale, N.A. Clark, J.E. Maclennan, M. Walsh, S.S. Keast, and M.E. Neubert, Phys. Rev. Lett. **82**, 2508 (1999).
[32] C. Da-Cruz, J.C. Rouillon, J. Marcerou, N. Isaert, and H.T. Nguyen, Liq. Cryst. **28**, 125 (2001).
[33] D. Schlauf, C. Bahr, and H.T. Nguyen, Phys. Rev. E **60**, 6816 (1999).
[34] L.S. Hirst, S.J. Watson, H.F. Gleeson, P. Cluzeau, P. Barois, R. Pindak, J. Pitney, A. Cady, P.M. Johnson, C.C. Huang, *et al.* Phys. Rev. E **65**, 041705 (2002).
[35] P.M. Johnson, S. Pankratz, P. Mach, H.T. Nguyen, and C.C. Huang, Phys. Rev. Lett. **83**, 4073 (1999).
[36] F. Gouda, K. Skarp, and S.T. Lagerwall, Ferroelectrics **113**, 165 (1991).
[37] P. Martinot-Lagarde and G. Durand, J. Phys. (France) **42**, 269 (1981).
[38] R. Douali, C. Legrand, V. Faye, and H.T. Nguyen, Mol. Cryst. Liq. Cryst. Sci. Technol., Sect. A **A 328**, 209 (1999).
[39] R. Douali, C. Legrand, and H.T. Nguyen, Ferroelectrics **245**, 101 (2000).